



On the Shear-Thinning of Alkanes

Hongyu Gao¹ · Martin H. Müser¹

Received: 19 September 2023 / Accepted: 21 November 2023
© The Author(s) 2023

Abstract

The approximate power law dependence of the apparent viscosity of liquids on shear rate is often argued to arise from a distribution of energy barriers. However, recent work on the Prandtl model, which consists of a point mass being dragged by a damped, harmonic spring past a sinusoidal potential, revealed a similar dependence of the friction on velocity as that of many liquids. Here, we demonstrate that this correlation is not only qualitative but can also be made quantitative over a broad temperature range using merely three dimensionless parameters, at least for alkanes, in particular *n*-hexadecane, at elevated pressure *p*. These and other observations made on our all-atom alkane simulations at elevated pressure point to the existence of an elementary instability causing shear-thinning. In addition, the equilibrium viscosity shows power law dependence on *p* near the cavitation pressure but an exponential dependence at large *p*, while the additional parameter(s) in the Carreau–Yasuda equation compared to other rheological models turn out justifiable.

1 Introduction

Research on how liquids oppose shear as a function of shear stress or shear rate, temperature, and also pressure supposedly started almost exactly a century ago [1], when Schalek and Szegvari [2] discovered that the apparent viscosity η of iron-oxide colloidal suspension, defined as the ratio of shear stress τ and shear rate $\dot{\gamma}$, became continuously smaller with increasing shear rate. Ostwald [3] soon found that this shear-thinning, termed “Strukturviskosität” at the time (structure or intrinsic viscosity in English), can be approximated rather well with an $\eta \propto \dot{\gamma}^{n-1}$ power law, where *n* is called the shear-thinning exponent. It is now well established that any liquid, even the prototypical Newtonian fluid water when supercooled [4], has a shear rate dependent viscosity if the shear rate is only sufficiently high so that labeling fluids as (approximately) Newtonian or not is not a matter of chemistry but mostly of shear rate. Liquids obeying Ostwald’s empirical law with $n > 1$, $n = 1$, and $n < 1$ can be labeled shear-thickening, Newtonian, and shear-thinning, respectively. Under certain situations, $n < 0$ might be observable, in which case the friction force decreases with velocity, e.g., in computer simulations of poly- α -olefins and

2,4-dicyclohexyl-2-methylpentane at shear rates exceeding 1 GHz [5]. However, macroscopic flow could not be Couette like in such situations, because unavoidable fluctuations of the laminar flow profile would instantly grow, thereby resulting in a dynamical instability producing narrow zones of large slip.

The equilibrium viscosity $\eta_0(T, p)$ generally increases with pressure *p* and decreases with temperature *T* [6, 7]. One central reason for this behavior certainly is that elevating pressure makes it more difficult for molecules to move past each other, mainly because of increased steric repulsion, while higher temperature assists molecules to overcome energy barriers, whereby shear flow is facilitated. The functional form of $\eta(\dot{\gamma})$, e.g., the exponent *n* in (post-) Ostwald shear-thinning laws, evolves rather smoothly with pressure and temperature with potential exceptions occurring in the vicinity of a liquid-liquid phase transformation. This has enticed researchers to estimate effective viscosities at temperatures, pressures, and shear rates that are difficult to access experimentally using time-temperature and pressure superposition principles [8], similar to those used for the construction of master curves describing the linear viscoelasticity of rubbers or glass-forming liquids [9].

It remains actively debated what shear-thinning model describe real-laboratory or *in-silico* experimental data the best [10]. For example, Bair et al. [11] objected to the validity of the Eyring model [12] to describe rheological data, which had been advocated by Spikes and Jie [13, 14]. In a

✉ Martin H. Müser
martin.mueser@mx.uni-saarland.de

¹ Department of Materials Science & Engineering, Saarland University, Campus C6 3, 66123 Saarbrücken, Germany

possible retaliation, Spikes [15] dismissed work by Voeltzel, Vergne et al. [16, 17] on the rheology of ionic liquids with variable shear-thinning exponent, by favoring the Eyring model over the originally used Carreau model [18]. (These and related models are introduced in Sect. 2). Also the question what (simple) theory provides the best microscopic explanation for shear-thinning in fluids remains discussed, e.g., whether Eyring's [12] or Prandtl's [19] approach is more appropriate [20], although it seems often unappreciated that Prandtl had already worked out Eyring theory as a limiting case of his model and that Eyring admitted his results to be similar to Prandtl's and related prior work.

Another debate evolves around the question what time-temperature, or even time-temperature-pressure superposition principle is best suited for lubricants. For example, Bair [21] objected to the cross-over from a non-Arrhenius to an Arrhenius dependence of the viscosity upon cooling that Jadhao and Robbins had claimed to have identified for squalane [22, 23], though it seems that the transition from non-Arrhenius to Arrhenius dependencies of viscosity and diffusivity, which in some cases is called a fragile-to-strong transition, is a generic phenomenon of glass-forming melts [24].

In this work, we revisit the dependence of the viscosity of simple liquids depends on shear rate, temperature, pressure and molecular weight. While numerous simulation studies [8, 22, 25–27] have computed $\eta(\dot{\gamma})$ relations for realistic lubricant models in the past, often with the attempt to correlate molecular rearrangement with shear-thinning [27], see Ref. [10] for a recent review, we focus here on the question if the similarity of shear-thinning in realistic model liquids and that observed in the Prandtl model [19] are merely qualitative in nature or if they could be quantitative. To this end, we generate a reference relation of $\eta(\dot{\gamma})$ for hexadecane at $T = 500$ K and a hydrostatic pressure of $p = 300$ MPa and identify a Prandtl model that reproduces the $\eta(\dot{\gamma})$ relationship satisfactorily for that reference. Next, either temperature or pressure or the molecular weight of the alkane is varied and the changes in equilibrium viscosity studied and discussed in the framework of the Prandtl model. It had been introduced as a simple model for dislocation motion and argued to also explain the velocity dependence of solid friction or the shear-thinning of fluids, around similar times when shear-thinning was reported for the first time [19, 28].

In this investigation, we mean to understand trends rather than to produce accurate numbers for specific molecules. To this end, we study relatively low-viscosity liquids and relatively small compressive stresses, because we would not be in a position to compute equilibrium viscosities of technologically relevant poly- α -olefins (PAO) at Gigapascal (GPa) pressures within the statistical accuracy needed for our purposes. In fact, it remains a challenge to accurately

determine viscosities of PAOs from simulations even at ambient conditions and experimentally at $P > 5$ GPa [29]. Nonetheless, we see computer simulation as an ideal tool to rationalize trends, because high shear rates can be reached while conditions such as shear rate, pressure, and temperature can be set to a target precision. Moreover, undesired effects like frictional heating can be suppressed or at least be quantified. Last but not least, the pressure-dependence of the viscosity can be investigated even under a well-defined isotropic, tensile stress.

We continue this paper with a background section on rheological models in Sect. 2. Theory and numerical methods are introduced in Sect. 3. Results are presented in Sect. 4, while conclusions are drawn in Sect. 5.

2 Background on Rheological Models

The rheology of a broad class of different liquids including standard base oils, water, or blood is captured quite well by the Carreau-Yasuda (CY) equation,

$$\eta(\dot{\gamma}) = \eta_{\infty} + (\eta_0 - \eta_{\infty}) \left\{ 1 + (\dot{\gamma}/\dot{\gamma}_0)^a \right\}^{(n-1)/a}, \quad (1)$$

where η_0 is the equilibrium viscosity, $\dot{\gamma}_0$ is a reference shear rate, near which shear-thinning starts or has started to set in, while η_{∞} is a parameter discussed in detail in the next paragraph. Two other popular models arise as limiting cases of Carreau-Yasuda, namely the Carreau model [18] for $a = 2$ and the Cross model [30] for $a = 1 - n$.

An arguably tricky term in Eq. (1) is the large-shear rate limit of the viscosity, η_{∞} , even if it is often useful to introduce it in practice so that fitting functions extend their validity to large shear rates. However, at the point at which $\eta(\dot{\gamma})$ appears to level off, the way in which stress and temperature are controlled is likely to matter. For example, we find that fitting viscosity data when reported for constant (mean) pressure as a function of $\dot{\gamma}$ does not require η_{∞} to be introduced, while it does at constant-density. These observations are in line with classical results by Daivis and Evans [25], who found decane to show a finite value of η_{∞} or even to shear thicken at constant-density simulations but not at constant pressure. For these reasons, η_{∞} will be ignored in the following, all the more extreme shear-thinning at very large $\dot{\gamma}$ is readily built-in and thus rationalized in the Prandtl model, see Sect. 3.1.

Coming back to the discussion of rheological models: Carreau [18] had originally attempted to simultaneously address the linear-response viscoelasticity and the out-of-equilibrium shear-thinning by assuming the rates of creation and annihilation of molecular junctions to be functions of what now would be called the equivalent von Mises strain-rate. Carreau suggested two *ad-hoc*

functional dependencies for those functions, one of which he dismissed as unrealistic, which, ironically is the one leading to the equation, which is now popular and carries his name, i.e., Eq. (1) for $a = 2$.

A beneficial aspect of the Carreau model is that the leading-order corrections to the linear-response viscosity are, as they should be, of order $\dot{\gamma}^2$ [31]. However, it seems that expanding the Carreau equation into (even) powers of the shear rate does not accurately reflect the initial but only the later deviations of the viscosity from the equilibrium viscosity. We base this conclusion on the observation that almost any high resolution data that we are aware of, be it experimental or simulations, lies below the fits at the point where η has decreased to say 80% its equilibrium value.

Another shear rate dependence of the viscosity, which can be motivated from Eyring theory, is

$$\frac{\eta}{\eta_0} = \frac{\dot{\gamma}_0}{\dot{\gamma}} \operatorname{asinh}\left(\frac{\dot{\gamma}}{\dot{\gamma}_0}\right), \tag{2}$$

where the ideal value for $\dot{\gamma}_0$ may differ from that of another rheological model. This relation makes the shear stress increase logarithmically with $\dot{\gamma}$ at large $\dot{\gamma}$ while converging to the equilibrium viscosity η_0 at $\dot{\gamma} \rightarrow 0$, as is typical for elstohydrodynamic lubrication. This is arguably the main reason for the use of this and related relations in state-rate models of frictional contacts [32]. However, what appears to be often overlooked is that Eq. (2) can be seen as a limiting case of Eq. (1), because an increase of shear stress or friction with a power-law $\dot{\gamma}^\epsilon$ with $0 < \epsilon \ll 1$ behaves essentially logarithmically. Thus, as long as $0 < n \ll 1$, discrepancies between Eyring and the other rheological models can only be minor, in which case the dominating advantage of Eyring would be to depend on merely two adjustable parameters.

When evaluating the functional form of a given model, mostly the viscosity and sometimes the shear stress or friction are often represented in a double logarithmic plot as a function of shear rate or velocity. This way differences between different models near the cross-over from Stokes friction to ‘‘Ostwald scaling’’ have a low optical resolution. It can be improved, in particular for shear-thinning exponents near ‘‘Eyring scaling’’, i.e., $0 < n \ll 1$, when multiplying the viscosity with the square-root of the shear rate [31, 33]. An example of such a plot, referred to in the following as an *intermediate scaling plot* is shown in Fig. 1. It contrasts the regular $\eta(\dot{\gamma})$ representation for the exponent $n = 0.2$ with an intermediate scaling plot. In this example, n was chosen roughly half way between the values identified in this study and $n = 1 - \epsilon$, $0 < \epsilon \ll 1$, at which point the algebraic dependence of shear stress on shear rate is logarithmic like.

To quantify the goodness of fits to molecular dynamics (MD) results, we defined a χ^2 -error as a logarithmic

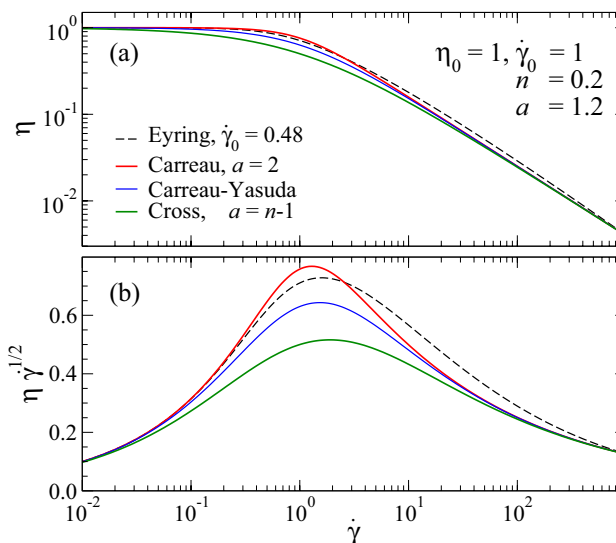


Fig. 1 Shear rate dependence of the viscosity η as produced by various model, (a) in a regular representation and (b) in an alternative fashion. All model functions assume the same linear-response viscosity η_0 and a similar $\eta(\dot{\gamma} = 10^3)$. Carreau-Yasuda (blue line), Carreau (red), and Cross (green) employ the same value for n and $\dot{\gamma}_0$

deviation of the viscosity function from the reference data, i.e.,

$$\chi^2 = \frac{1}{N} \sum_{n=1}^N \left\{ \ln \frac{\eta_{\text{model}}(\dot{\gamma}_n)}{\eta_{\text{MD}}(\dot{\gamma}_n)} \right\}^2, \tag{3}$$

where N enumerates the data points. This way, errors do not depend on whether stress or viscosity are targeted. To not bias the fits to large or low shear rates, we furthermore used $\dot{\gamma}_{n+1}/\dot{\gamma}_n$ constant.

3 Theory and Methods

3.1 Inertia-Free Prandtl Model

In the Prandtl model, a mass point is pulled with a spring over a corrugated substrate. In addition to the conservative forces, Stokes’ friction terms arise, which are argued to reflect lattice vibrations in the substrate. However, this explicit damping can also be assumed to occur in the pulling spring, in which case the mass point’s equation of motion in the presence of thermal noise $\Gamma_{\text{th}}(t)$ reads

$$\gamma_0(\dot{x} - v_0) = qV_0 \sin(qx) + k(x - v_0t) + \Gamma_{\text{th}}(t) \tag{4}$$

Here x is the position of the ‘‘Prandtl atom’’, \dot{x} its velocity, v_0 the velocity of the pulling spring, γ_0 is a damping term of unit kg/s, V the amplitude of the sinusoidal potential

through which the atom is dragged, $2\pi/q$ is the period of the potential, k the stiffness of the pulling spring, and Γ_{th} is thermal noise with the expectation values

$$\langle \Gamma_{th}(t) \rangle = 0 \tag{5}$$

$$\langle \Gamma_{th}(t)\Gamma_{th}(t') \rangle = 2\gamma_0 k_B T \delta(t - t'), \tag{6}$$

where $k_B T$ the thermal energy and $\delta(\dots)$ is the Dirac delta function. We have the liberty to use a unit system of our choice, i.e., one in which q , V_0 , and γ define the units used for inverse length, energy, and weight per time. When doing so, it becomes clear that this form of the Prandtl model has two parameters defining the shape of a $F(v)$ relation, since only the reduced stiffness $\tilde{k} \equiv k/(q^2 V)$ and the reduced temperature $\tilde{T} \equiv k_B T/V$ remain, in which case the dynamical equation to be solved, introducing $\langle \tilde{\Gamma}_{th}(t)\tilde{\Gamma}_{th}(t') \rangle = \delta(t - t')$, simplifies to

$$\dot{x} - v_0 = \sin x + \tilde{k}(x - v_0 t) + \sqrt{2\tilde{T}}\tilde{\Gamma}_{th}(t), \tag{7}$$

In this model, only two dimensionless numbers, \tilde{k} and \tilde{T} , determine the *shape* of a $\eta(\dot{\gamma})$ relation, e.g., the exponents n and a that would be obtained when fitting simulation data to a Carreau-Yasuda relation. Absolute values, such as the equilibrium viscosity η_0 or the cross-over shear rate $\dot{\gamma}_0$ are then determined by the model parameters defining the units in the Prandtl model. For example, given a value of \tilde{k} and assuming \tilde{k} and V_0 to be temperature-independent, the small-temperature dependency of the equilibrium-damping constant of the Prandtl model, which is proportional to the viscosity, reveals Arrhenius-type dependence [31] with the energy activation barrier ΔE whose construction is shown

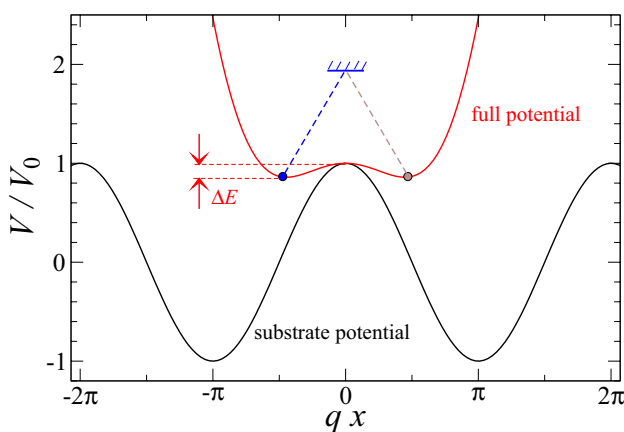


Fig. 2 Substrate and total potential energy for $\tilde{k} = 0.7$, which is used as the reference state (300 MPa, 500 K, which corresponds to $\tilde{T} = 0.076$). The energy barrier $\Delta E = 0.14$ is defined at the moment of time when the position of the driving spring coincides with the maximum of the substrate potential

in Fig. 2. Assuming the temperature to be below the liquid’s fragile-to-strong transition temperature and ΔE to be known, the unit for V_0 can then be fixed.

When varying temperature of a large range, it seems clear that both V_0 and k depend on temperature. Specifically, at large T , the all-atom liquid expands, which will reduce V_0 supposedly more than k . To reflect such effects of thermal dilation in the model, we allowed \tilde{k} to obey

$$\tilde{k} = \tilde{k}_\infty \exp(-T_k/T), \tag{8}$$

where T_k is an empirical parameter, which would need to get readjusted as a function of pressure and the degree of polymerization. The exponential dependence is motivated by the Boltzmann distribution without any further justification. However, we note that the value used for T_k was only $T = 90.5$ K, is clearly less than the smallest investigated temperature of 300 K.

Before discussing some important asymptotic limits of the Prandtl model, we wish to justify why we damp the spring motion rather than the velocity of an atom or rather a material point relative to the substrate. First, the kinetic energy of monolayers sliding across a substrate was shown to be related to the (anharmonic) coupling of vibrations in the monolayer [34] and we see a Prandtl spring to reflect the coupling of a central atom to its in-plane neighbors of a lamella during laminar flow. Second, damping relative to the substrate would yield a high-velocity damping, which would produce a finite η_∞ . However, as discussed in Sect. 2, we see no evidence for the existence of η_∞ , when evaluating $\eta(\dot{\gamma})$ such that volumes are adjusted for each run to yield the target pressure on average.

A few properties of the Prandtl model are worth reciting, most of which can be found in [35]. First, instabilities and thus (athermal) static friction and Coulomb-like friction at low temperatures can only occur when $\tilde{k} < 1$. Second, the athermal low-velocity limit of the friction-velocity relation reads $F_k - F_s \propto v^{2/3}$. Thus, for \tilde{k} being in the immediate vicinity of unity, a shear-thinning exponent of $n = 2/3$ is obtained. This value thereby constitutes an upper bound for what shear-thinning exponent n can be reproduced with the Prandtl model. Third, in the limit $0 < \tilde{k} \ll 1$, the material point is effectively moved with a constant force, which is the limit at which the Prandtl model corresponds to situation described by himself and later again by Eyring. In that limit, the effective damping at small but finite temperature can be described with Eq. (2). Thus, the Prandtl model can reproduce any shear-thinning exponent between $0 < n \leq 2/3$, where a small exponent would imply small \tilde{k} and/or finite temperature, while $n = 2/3$ would suggest thermal fluctuations to be minor and/or \tilde{k} to be relatively close to unity. In fact, the Prandtl model reproduces the general

trend of real lubricants [10] that n decreases with decreasing temperature [31].

The fourth asymptotic limit to be discussed is the high-velocity limit. In this case, the atom moves at constant velocity of v_0 plus small fluctuations, which can be described using perturbation theory. The first-order perturbation is a time-dependent force $qV \sin(\omega t)$ with $\omega = qv_0$. For $\omega \rightarrow \infty$, the response function $\tilde{x}_1(\omega) \propto 1/\omega$ so that the dissipated power $P \propto |\omega \tilde{x}_1|^2$ is independent of ω . This scaling means that the friction force is proportional to $1/\omega$ or $1/v$, which, when applied to laminar flow would translate to $n = -1$. Couette flow would no longer be possible, as discussed in the introduction. Adding inertia to the model would further impede Couette flow at large $\dot{\gamma}$ as \tilde{x}_1 would then be proportional to $1/\omega^2$ at large ω , which decreases n to $n = -3$. Irrespective of the choice of the mass, extreme shear-thinning at very high shear rate occurs in the Prandtl model, when the spring head moves so fast that the energy released during an instability can no longer be transferred into heat before the atom undergoes the next instability. We would argue that similar statements can be made for any other systems and degrees of freedom showing decreasing friction with increasing velocity.

3.2 Molecular-Dynamics Alkane Simulations

Non-equilibrium molecular dynamics (NEMD) simulations are carried out on a bulk liquid consisting of approximately 5,000 atoms using the open-source code—LAMMPS [36]. Interatomic interactions are modeled with the all-atom L-OPLS-AA force field [37, 38], which describes bond-stretching, bending, and torsional in addition to non-bonded interactions. The shear viscosity is calculated through Couette flow simulations, where shear flow is applied using the SLLOD algorithm [39] and ‘fix deform’ command, equivalent to the Lees-Edwards [40] periodic boundary conditions. The system temperature, $320 \text{ K} \leq T \leq 550 \text{ K}$ was maintained with a Nosé-Hoover thermostat [41, 42]. To this end, the LAMMPS command temp/deform was used that removes the effect of a mean velocity profile from the determination of kinetic energy and thus temperature.

Results are reported for a fixed normal pressure, which was achieved as follows: In a first set of short simulations at fixed volumes and shear rates, an equation of state for the give shear rate was ascertained and the volume determined by interpolation (never extrapolation!) at which the target pressure was expected to occur. This volume was then used in a longer run during which the effective viscosity was calculated. The average normal stress in those long runs always turned out within 1% at finite stress and $\pm 1 \text{ MPa}$ at zero stress, where small relative

errors are somewhat difficult to achieve. In the case of moderate, mean tensile stresses, the same average value σ_{33} value can be reached with two different densities.

4 Results

4.1 Temperature Dependence

We first investigate the dependence of the viscosity of hexadecane as a function of temperature at a pressure of $p_{33} = 300 \text{ MPa}$, where $p_{33} \equiv -\sigma_{33}$. The latter value was chosen such that it is high enough to almost represent boundary-lubrication conditions but small enough so that the equilibrium viscosity could be calculated down to a temperature of $T = 320 \text{ K}$, which would be at the cold end of engine oil after warming up. Figure 3 shows the raw data obtained from MD simulations and fits based on the Carreau-Yasuda equation.

The range of shear rates presented in Fig. 3 and others presented in this work is certainly beyond any practical relevance, which should be roughly $\dot{\gamma} = 1 \text{ GHz}$, obtained when two surfaces moving at a relative velocity of 2 m/s have a local separation of 2 nm . However, owing to time-temperature and time-pressure superposition principles, similar rheology (except for prefactors) can occur at “reasonable” shear rates when the temperature is lowered and/or the pressure increased. Nonetheless, using shear rates clearly above 10^{12} Hz would not be meaningful, because these rates exceed local librational frequencies.

Although it has been a matter of ongoing debates what functional form describes data as that presented in Fig. 3 best, we feel that an intermediate scaling plot allows

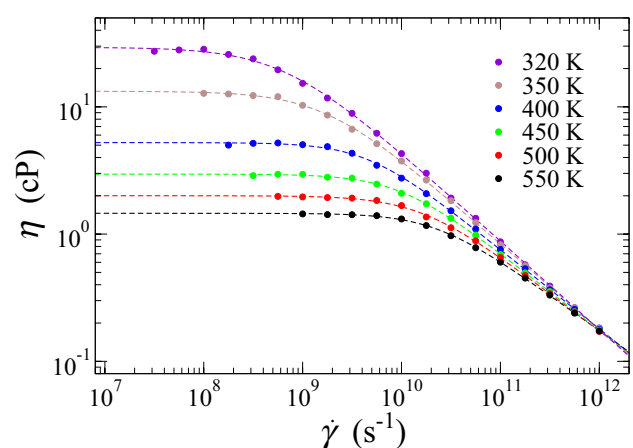


Fig. 3 Shear viscosity η of n -hexadecane as a function of shear rate $\dot{\gamma}$ at various temperatures (320–550 K) and fixed volumes yielding a mean normal pressure of 300 MPa for each data point. Symbols show NEMD data and dashed lines fits to the data using the Carreau-Yasuda equation

differences between fit and data to be much better resolved than traditional representations of $\eta(\dot{\gamma})$. For the data in question, our results for viscosity spanning two decades in a regular $\eta(\dot{\gamma})$ representation as in Fig. 3 vary merely by a factor of about three in the cross-over domain, as can be seen in Fig. 4. This improves the resolution of the graph substantially, whereby both small deficiencies of rheological model or stochastic errors are relentlessly revealed.

Figure 4 compares three rheological models for the viscosity of hexadecane at three different temperatures. It can be seen by the naked eye that the Eyring model produces the data in the least satisfactory manner. Carreau is a substantial

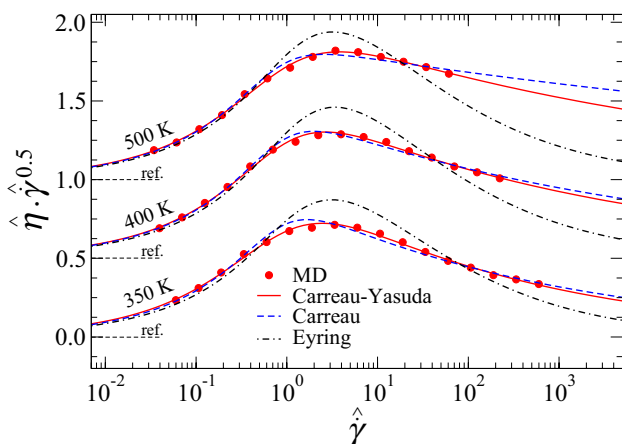


Fig. 4 A comparison of phenomenological models fitted to a representative case of *n*-hexadecane at $T = 350, 400,$ and 500 K and $p_{33} = 300$ MPa with normalized $\hat{\gamma} = \dot{\gamma}/\dot{\gamma}_0^{CY}$ and $\hat{\eta} = \eta/\eta_0^{CY}$, where the upper index CY indicates that the Carreau-Yasuda values at the given values were taken as units for viscosity and frequency. Results from $T = 400$ K and 500 K are shifted in y direction by 0.5 and 1.0 , respectively

improvement to Eyring, however, Carreau overestimates the viscosity at shear rates slightly lower than the maximum. We invite readers to check for this deviation to occur in other published data and invite them to remember our assessment that this short-coming of Carreau shows up in the early shear-thinning regime the more clearly the less noisy the real-laboratory or *in-silico* data.

Relative standard-deviations converted in percentages, $\chi\% \equiv 100 \cdot \chi$, are listed in Table 1 for all rheological models introduced in this paper so far and all MD-based $\eta(\dot{\gamma})$ reference data. The latter includes data obtained by varying the pressure or the molecular weight rather than the temperature from their default values.

Since Carreau (Ca) and Cross (Cr) are exact limits of Carreau-Yasuda (CY), they cannot outperform CY. It is similarly clear that Eyring (E) should be the least accurate of the four models, because it arises as an approximate asymptotic limit from the other models. However, the interesting question is to what degree increasing the number of fit parameters from 2 (E) to 3 (Ca, Cr) to 4 (CY) improves the goodness of the fits. Our personal view is that the dividing line between justified and unjustified additional parameter is a reduction of χ by a factor that should be clearly smaller than $k/(k + 1)$ when k is the number of originally adjustable coefficients.

Table 1 reveals quite clear trends. Errors associated with Eyring exceed 10% in all but three out of 15 sets of simulations. The Cross model reduces the errors compared to Eyring by a factor always exceeding 1.9 and in the clear majority of cases by a factor greater than 2.5. Thus, the additional adjustable parameter seems justified. Carreau further reduces the error compared to Cross quite substantially, except at the highest temperature and the lowest pressure reported in Table 1. Carreau-Yasuda is again a clear improvement on Carreau. Improvements scatter between

Table 1 Results for Carreau-Yasuda (CY) fits to MD data. P stands for the number of backbone carbons. Relative standard-deviations are also included for fits to Carreau (C), Cross (Cr), and Eyring (E)

P	T/K	p_3/MPa	η_0/cP	$\dot{\gamma}_0/\text{GHz}$	n	a	$\chi_{CY}\%$	$\chi_C\%$	$\chi_{Cr}\%$	$\chi_E\%$
16	350	300	26.76	0.71	0.310	1.28	4.12	5.45	6.46	17.77
			13.25	1.67	0.327	1.17	1.93	4.11	4.56	15.78
			5.24	4.50	0.376	1.42	1.86	2.79	5.41	13.73
			2.96	9.65	0.391	1.34	1.25	2.67	4.53	11.53
			2.00	16.37	0.406	1.25	1.65	3.00	3.71	10.64
			1.46	22.35	0.441	1.36	0.97	2.06	3.51	9.96
16	500	100	0.66	59.25	0.300	1.16	1.61	3.29	2.41	4.66
			1.20	26.37	0.404	1.35	1.67	2.58	3.69	8.03
			2.00	16.37	0.406	1.25	1.65	3.00	3.71	10.64
			2.97	9.66	0.425	1.45	1.74	2.44	5.00	12.63
			4.36	7.61	0.398	1.26	1.84	3.16	4.38	13.47
			5.90	5.31	0.404	1.45	1.07	2.14	5.45	14.46
16	500	300	2.00	16.37	0.406	1.25	1.65	3.00	3.71	10.64
			2.81	8.54	0.421	1.32	1.77	2.88	4.61	13.62
24			3.83	5.26	0.418	1.19	1.97	3.53	4.51	16.26

reduction factors of 1.3 and 2.2, however, the median improvement in the reported data lies at about 1.8. For this reason, we judge the extra parameter a in Carreau-Yasuda as significant, in particular as the Carreau-Yasuda errors are often only marginally larger than the statistical uncertainty of the produced data. Unfortunately, it is beyond our current resources to substantially reduce the thermal/statistical errors, because halving statistical errors implies quadrupling the numerical effort.

While all investigated model functions, even that based on Eyring, matches the MD data in the representation of Fig. 4 substantially better than an “arbitrary fitting function”—such as a skewed Gaussian, which, like Carreau-Yasuda, has four adjustable parameters—Cross, Carreau, and Carreau-Yasuda are purely heuristic functions with built-in linear-response at small shear rates and power law dependence at large shear rates. However, unlike Eyring and even more so Prandtl, they lack a clear microscopic justification. The Prandtl model is a physics-based model, in which linear-response at small velocities arises naturally while quasi-power law behavior occurs at large shear rates [28, 31].

The just-mentioned feature of the Prandtl model motivated us to explore to what extent the two dimensionless parameters of the Prandtl model can be tuned to match experimental or realistic, *in-silico* data. The interesting aspect of such an analysis is that the model parameters can be fixed at one temperature and changes in $\eta(\dot{\gamma})$ be estimated without requiring adjustment of the parameters beyond including a smooth temperature dependence of \tilde{k} .

Figure 5 reveals that three dimensionless parameters and thus a total of five parameters is sufficient to reproduce the full-scale NEMD results at different temperatures. Interestingly, it also reproduces the observation that the exponent n decreases thereby approaching Eyring-like behavior with

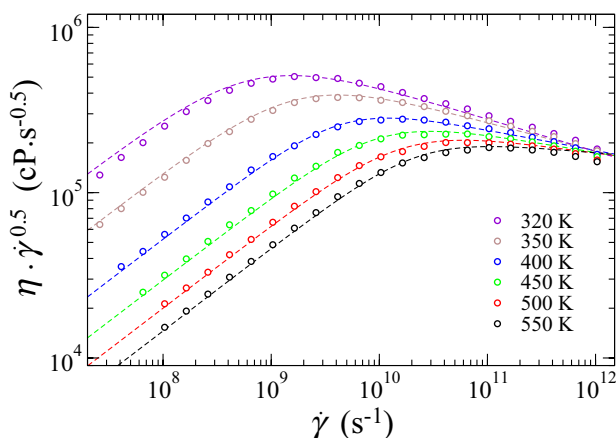


Fig. 5 Comparison of results obtained from the Prandtl model to Carreau-Yasuda fits to the hexadecane MD results at $p_{33} = 300$ MPa (dashed curves). The Prandtl model was chosen with $\tilde{k} = 0.84 \cdot (1 - 90.5 K/T)$ and $\tilde{\tau} = 1.52 \cdot 10^{-4} T/K$

decreasing temperature. Specifically, the full simulations show $n = 0.391$ at $T = 450$ K and $n = 0.327$ at $T = 350$ K, while the Prandtl model finds $n = 0.366$ and 0.321 at those two temperatures, respectively. Thus, the Prandtl model does not perfectly reproduce the reduction in the shear-thinning exponent but supposedly much better than expected from a simple model.

Figure 6 further reveals the large degree of correlation between the results of all-atom simulations and those of the Prandtl model. Both data sets have the same inverse correlation of η_0 and $\dot{\gamma}_0$, as would be expected from the equilibrium dynamics of an activated process.

The final analysis in this section is concerned with the temperature dependence of hexadecane’s viscosity at the relatively large, constant compressive stress of $p_{33} = 300$ MPa.

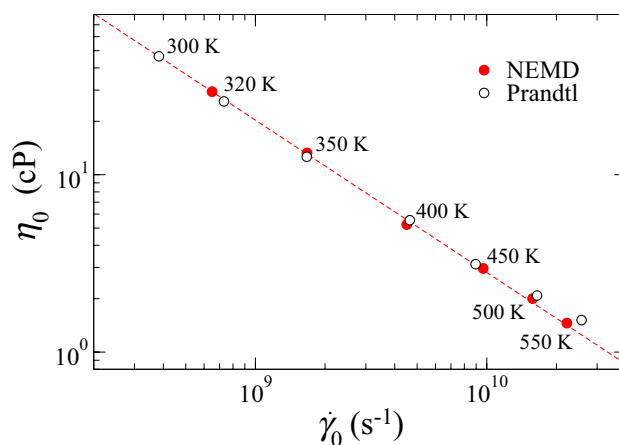


Fig. 6 Relation between equilibrium viscosity η_0 and cross-over shear rate $\dot{\gamma}_0$ as obtained in full NEMD simulations and the Prandtl model. The dashed line reflects a slightly sublinear, inverse power law, i.e., $\eta_0 \propto 1/\dot{\gamma}_0^{0.84}$, which is drawn to guide the eye

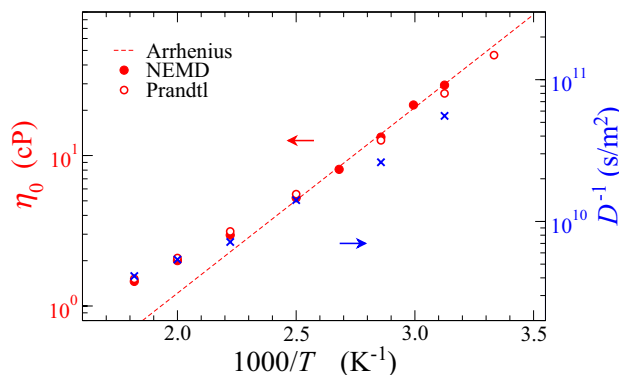


Fig. 7 Newtonian viscosity η_0 from all-atom simulations (full, red circles) and Prandtl model (open, red circles) and inverse diffusion coefficient $1/D$ of hexadecane (blue crosses) as a function of inverse temperature, for n -hexadecane, at 300 MPa. Both ordinates, i.e., η_0 on the left and $1/D$ on the right, span the same factor of 100

Figure 7 hints to a cross-over from a non-Arrhenius to an Arrhenius-like dependence in the all-atom MD data. Unfortunately, some doubt on the robustness of the Arrhenius-type dependence at small-temperature remains, as we have not yet managed to compute an equilibrium viscosity below 320 K within our statistical error margin of about 1% from the full MD simulations. However, the Prandtl model, which accounts for the cross-over reasonably well, while clearly having a constant energy barrier supports an extension of an Arrhenius dependence to smaller temperature. The model thereby also reveals that the deviation from Arrhenius at large T might not be caused by temperature-dependent energy barriers but could be owing to the ratio $\Delta E/k_B T$ not being a large number, at which point the exponential factor $\exp(\Delta E/k_B T)$ no longer dominates other temperature dependencies.

In order to explore if there is a FST, we computed the diffusion coefficient D of carbon atoms from their time-dependent root-mean-square displacement (see also Sect. 4.4 for a more detailed discussion) to see if the temperature dependence of the diffusion coefficient starts to decouple from that of the viscosity, as it happens at the FST of glass-forming melts. Figure 7 provides some evidence for this to happen, which, however is relatively weak, because accurate diffusion coefficients at small-temperatures are difficult to determine. Thus, more research, which is currently outside the scope of our computational feasibility, is required to see if (a) the viscosity is really Arrhenius-like at small-temperature and (b) if the cross-over can already be rationalized within the Prandtl model or is in need of a more elaborate explanation like the FST. The difficulty is that statistical error bars are small at relatively small times, at which point the functional form used to fit the time-dependent root-mean-square displacement affect the value for D , while stochastic errors are large at large times. Thus, values for $1/D$ reported at the lowest temperatures must be taken with a grain of salt and might increase by roughly 20% with different fitting procedures than those that we assumed.

4.2 Pressure-Dependence

Besides the temperature dependence of the viscosity η at fixed pressure p_{33} , we also analyzed $\eta(p)$ at fixed temperature. This time, however, we present the results in the form of shear stress τ as a function of shear rate $\dot{\gamma}$, see Fig. 8. Results are also reported for simulations at a negative normal pressure. They reflect meta-stable conditions, because a thermally or shear-induced void in the liquid would unavoidably grow indefinitely under a tensile load once the void surpasses a critical nucleation size. However, including tensile stresses into the analysis allows us to explore the pressure-dependence on viscosity at values of p_{33} , where this dependence is particularly steep.

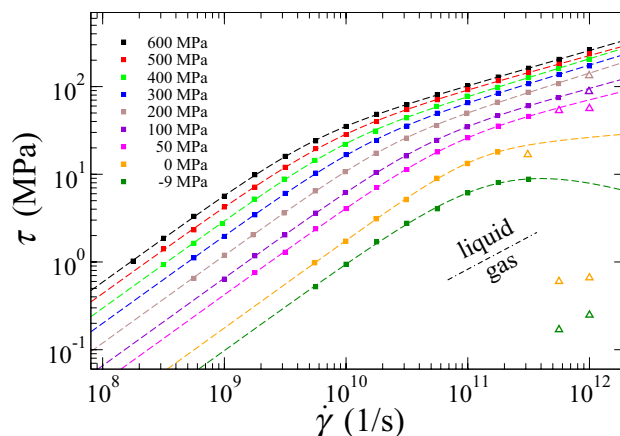


Fig. 8 Shear stress τ of n -hexadecane at various pressures (-9 – 600 MPa) and a constant temperature of 500 K. Symbols show NEMD data and dashed lines fits to it using the Carreau-Yasuda equation. At high shear rates, the system can be either in the liquid or in the gas-phase. Open symbols refer to the gas phase as well as data for the liquid phase, if some configurations exhibited shear localization

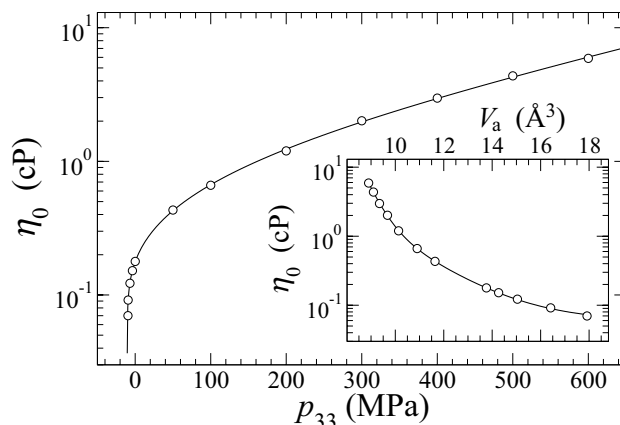


Fig. 9 Main graph: Newtonian viscosity η_0 of n -hexadecane as a function of normal pressure p at 500 K. Symbols show numerical results, while the line is a fit to Eq. (9). Inset: η_0 as a function of the volume V per atom. The line is a fourth-order polynomial of $\ln \eta_0$ in V

Analysis of the equilibrium viscosity, see Fig. 9, reveals that η_0 might disappear as a power law at a negative pressure of $p^* = -10.5$ MPa. This value is close to the pressure at which the volume of a meta-stable liquid, having been “stress-quenched” to a negative pressure, is expected to diverge. However, at large pressure, $\eta(p)$ crosses over to an exponential-like dependence of pressure. A simple functional form reflecting this behavior is

$$\eta(p) = \eta_1(p/p^* - 1)^\mu + \eta_2(e^{\beta p V^*} - e^{\beta p^* V^*}), \quad (9)$$

where the parameters η_1 , η_2 , μ , and V^* are phenomenological adjustable parameter and $\beta = 1/k_B T$ can be interpreted as

$V^* \approx \partial \Delta E / \partial p$ at intermediate pressures and be called “free volume”, even if it is not clear how to define or identify points belonging to free volume given atomic coordinates of a bulk liquid. The inset of Fig. 9 shows the viscosity as a function of volume. No extended domain of a linear $\ln \eta_0$ versus volume can be detected.

A few more words on the decrease of viscosity at $p \gtrsim p^*$ may be in place. The line represented in Fig. 9 is based on an exponent $\mu \approx 2/9$. However, the uncertainty of the exponent is rather large, as the value changes quite substantially depending on what data are included during the fitting. (We excluded the point at the lowest pressure.) Here, we would only want to state a rough upper bound of 1/2 for the exponent. Moreover, we would argue that the decrease in viscosity arises from a much reduced steric repulsion as molecules slide past each other under a tensile hydrostatic stress.

We do not intend to claim that the functional form of $\eta(p)$ proposed in Eq. (9) is superior to other descriptions, in particular generalizations of the McEwen equation [43], for example that by Bair [44] or others discussed recently by Kondratyuk, Pisarev, and Ewen [45]. While our analysis is suggestive of a quasi-exponential pressure-dependence at large compression might be an appropriate description, at least at low shear rates, such extrapolations are risky. Indeed, there is much evidence for super-exponential viscosity increase at very high pressure [46].

In fact, we find the McEwen $\eta(p)$ dependence, which can be cast as the $\eta_2 = 0$ limiting case of Eq. (9) to hold extremely well at compressive stress and fixed, large shear rates, as is demonstrated in the main part of Fig. 10. Here η_{neq} is the effective viscosity at a high shear rate and zero normal stress, the exponent μ is set to $\mu = 1/2$, and σ_0 a hypothetical tensile stress at which the McEwen formula

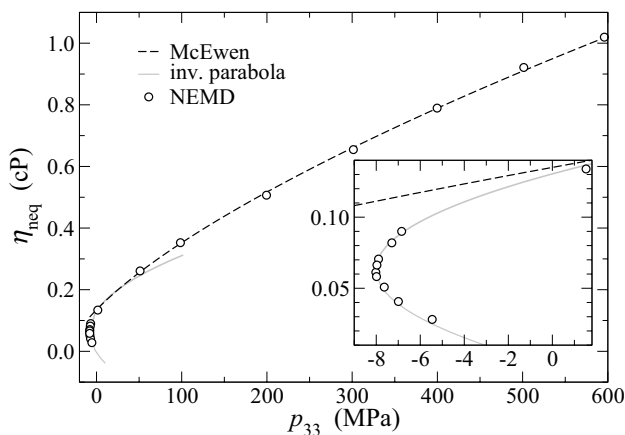


Fig. 10 Effective viscosity at a high shear rate of $\dot{\nu} = 10^{11}$ Hz at $T = 500$ K as a function of pressure p_{33} . The inset highlights result for tensile stresses

would predict the viscosity to disappear. (Using $\mu = 1/2$ substantially worsened the agreement between fit and data.) However, without further modification, the McEwen equation makes poor predictions once the stress becomes tensile, as can be seen in the inset of Fig. 10.

4.3 Chain-Length Dependence

In addition to changing pressure and temperature, we also altered the degree of polymerization, P , however, only in a relatively narrow range in which molecules are much too short to entangle. From the results reported in Table 1, it can be seen that η_0 and $\dot{\gamma}_0$ scale roughly with P^2 and $1/P^2$, respectively. Changes in the exponents n and a are rather small, which points once more to the existence of an elementary instability. This result does not necessarily contradict findings by Sivabeak and Persson (SP) [26], who suggested a more noticeable $n(P)$ dependence, where their symbol n corresponded to our $1 - n$. Further, more substantial difference between their and our study are that SP simulated the boundary-lubrication regime rather than bulk viscosities. Moreover, they explored a relatively small normal pressure of 10 MPa while altering P by a factor of 70, which covers the range from oligomer to entangled polymers.

An interesting feature born out in our data are that $\eta(\dot{\gamma})$ overlaps at very high shear rates for different degree of polymerization P , i.e., not only the exponent n but also the prefactors are similar at high shear rates for different alkanes (Fig. 11).

4.4 Microscopic Analysis

Since the early days of shear-thinning studies, attempts were made to rationalize phenomenological relations in

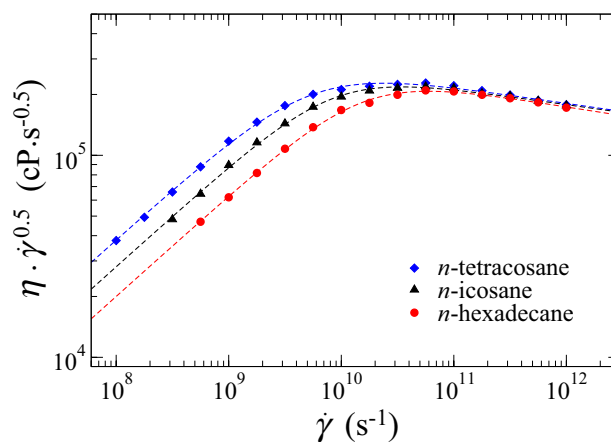


Fig. 11 Intermediate scaling plot of n -hexadecane, n -icosane, and n -tetracosane at 500 K and 300 MPa

terms of microscopic models and to relate shear-thinning to structural changes [47]. Early theories of polymers in solution [48], “derive” the Carreau equation by considering the rate of formation and breaking of contact points. Even if the explanation were valid for such systems, it can scarcely matter for dense polymer mixtures, when the resistance to flow is largely affected by steric repulsion. Yet, non-local configurational changes like polymer alignment have been held responsible for changes in viscosity [49]. Specifically, polymers oriented along the shear flow direction were expected to counteract shear in that direction than those with quasi-spherical equilibrium shapes.

It might have come as a surprise to many when Jadhao and Robbins [49] reported the alignment of polymers to have saturated when the viscosity had merely changed by a factor of two, which, in their master plot was at the very beginning of the shear-thinning regime. We can confirm their finding in our work but notice that molecules coil up again at very high shear rates when the volume is not kept constant but readjusted such that the mean normal pressure equals the target value. Thus, Ostwald scaling may occur even if the overall molecular shape develops in a non-monotonic fashion (Fig. 12).

For reason of completeness, we also present data that we produced to determine the diffusion coefficient from equilibrium simulations in Fig. 13. It shows the atom averaged mean-square displacement as a function of time. Unfortunately, the value for the diffusion coefficient is sensitive to what functional form is used when fitting to the dependence of the mean-square displacement $MSD(t) = \langle \{x(t) - x(0)\}^2 \rangle$ as a function of time. Assuming $MSD(t)$ to be a constant plus Dt at large times yields slightly

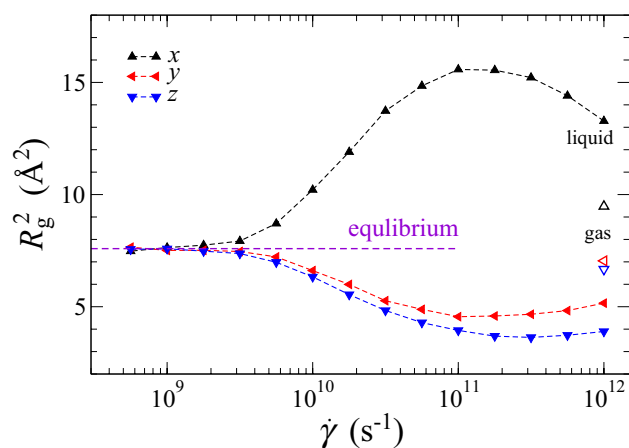


Fig. 12 Different Cartesian components to R_g^2 vs shear rate, for *n*-hexadecane at $p = 300$ MPa and $T = 500$ K (full symbols). Open symbols refer to gas-phase data at $p = 3.4$ MPa

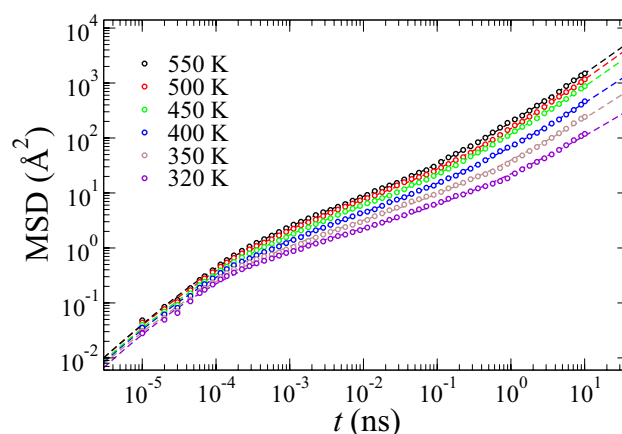


Fig. 13 Mean-squared displacement (MSD) of *n*-hexadecane from equilibrium MD simulation at 300 MPa. Lines are drawn to guide the eye

different results than when using the sum of a sub-diffusive and a diffusive function.

The calculations shown in Fig. 13 had been conducted to check if the cross-over from non-Arrhenius to Arrhenius is associated with a (collective) fragile-to-strong transition (FST) in a glass-forming melt, the (inverse) diffusion coefficient, $1/D$, was computed and the data included into Fig. 7. Both viscosity and inverse diffusion coefficient show rather similar scaling. Therefore, we do not see strong evidence that the cross-over from non-Arrhenius is associated with an FST. The weak temperature dependence of the effective hydrodynamic radius, R_H defined through the Stokes-Einstein relation, $D_0 = k_B T / (6\pi\eta_0 R_H)$ cannot be related to changes of the radius of gyration: while the hydrodynamic radius decreases by a factor of two, from $R_H \approx 1.08$ nm at the highest temperature $T = 550$ K to $R_H \approx 0.44$ nm at the lowest temperature $T = 320$ K, marginal increases were detected for R_g from $R_g(550 \text{ K}) \approx 0.475$ nm to $R_g(320 \text{ K}) \approx 0.494$ nm upon cooling. Thus, for our rather short chains, the ratio $X \equiv R_H/R_G$ falls from $X \approx 2.3$ to $X \approx 0.89$, which is greater than but of similar order of magnitude as $X = 0.664$, which is theoretically predicted for polymers in theta-solvents [50] or the X -ratios for various polymers in different solvents in the range of $0.5 \lesssim X \lesssim 1$ [51]. Interestingly, Prentice et al. [29] found a much more dramatic decrease in X for poly- α -olefins with increasing pressure than we found with decreasing temperature, though the trend of X becoming smaller as the ratio of energy barriers and thermal energy increases is identical.

5 Discussion and Conclusions

This work demonstrates that the shear-thinning of alkanes at small to medium pressures can be mapped quite well onto the Prandtl model. Fixing its two dimensional parameters at a given temperature and pressure even allows changes in the equilibrium viscosity and the functional form of $\eta(\dot{\gamma})$ to be reproduced over a reasonably broad temperature range without readjusting parameters. To a large degree, the parametrization is even transferable between different alkanes. Moreover, the obtained activation barrier of $\Delta E \approx 0.08$ eV that we obtain at a pressure of $p = 300$ MPa is greater but of similar order of magnitude as experimental result for the relaxational dynamics in polyethylen melts at zero pressure, which are close to 0.05 eV at ambient pressure [52]. Despite this success, we do not claim our parametrization to be optimal but rather minimal in the sense that the smallest number of adjustable parameters needed to describe shear-thinning was used. In principle, it could be attempted to also target the linear-response frequency dependence $\eta(\omega)$ by introducing a memory kernel into the damping coefficient.

Our simulation data on all-atom alkanes, in particular *n*-hexadecane also indicates that the additional parameter(s) used in a Carreau-Yasuda fit are justified, at least at elevated pressure. We find a fit to have a median error of roughly 12%, which reduces to about 6% when using an additional parameter in the Cross model. This error is cut once more into one half when using Carreau instead of Cross, and by almost another factor of two with Carreau-Yasuda, at which point the systematic error is almost on par with the stochastic error of the reference data.

Acknowledgements We thank Jörg Baschnagel and Daniele Dini for useful discussions.

Author Contributions MHM designed and supervised the project, wrote the manuscript. HG carried out all the simulations, analyzed the data and prepared the figures. MHM and HG reviewed and modified the manuscript.

Funding Open Access funding enabled and organized by Projekt DEAL. This research was supported by the German Research Foundation (DFG) under grant number GA 3059/2-1.

Data Availability Statement Data supporting the findings of this work are available upon request.

Declarations

Conflicts of interest The authors declare no competing interests.

Open Access This article is licensed under a Creative Commons Attribution 4.0 International License, which permits use, sharing, adaptation, distribution and reproduction in any medium or format, as long as you give appropriate credit to the original author(s) and the source, provide a link to the Creative Commons licence, and indicate if changes

were made. The images or other third party material in this article are included in the article's Creative Commons licence, unless indicated otherwise in a credit line to the material. If material is not included in the article's Creative Commons licence and your intended use is not permitted by statutory regulation or exceeds the permitted use, you will need to obtain permission directly from the copyright holder. To view a copy of this licence, visit <http://creativecommons.org/licenses/by/4.0/>.

References

- Barnes, H.A.: Thixotropy—a review. *J. Non-Newton. Fluid Mech.* **70**(1–2), 1–33 (1997)
- Schalek, E., Szegvari, A.: Die langsame koagulation konzentrierter eisenoxydsole zu reversiblen gallerten. *Kolloid-Zeitschrift* **33**(6), 326–334 (1923)
- Ostwald, W.: Ueber die geschwindigkeitsfunktion der viskosität disperser systeme. i. *Kolloid-Zeitschrift* **36**(2), 99–117 (1925)
- de Almeida, R.I., de Koning, M.: Non-Newtonian flow effects in supercooled water. *Phys. Rev. Res.* **2**(2), 022004 (2020)
- Ewen, J.P., Gao, H., Müser, M.H., Dini, D.: Shear heating, flow, and friction of confined molecular fluids at high pressure. *Phys. Chem. Chem. Phys.* **21**, 5813–5823 (2019)
- Bair, S., Kottke, P.: Pressure-viscosity relationships for elastohydrodynamics. *Tribol. Trans.* **46**(3), 289–295 (2003)
- Roland, C.M., Bair, S., Casalini, R.: Thermodynamic scaling of the viscosity of van der waals, h-bonded, and ionic liquids. *J. Chem. Phys.* **125**(12), 124508 (2006)
- Bair, S., McCabe, C., Cummings, P.T.: Comparison of nonequilibrium molecular dynamics with experimental measurements in the nonlinear shear-thinning regime. *Phys. Rev. Lett.* **88**, 058302 (2002)
- Li, R.: Time-temperature superposition method for glass transition temperature of plastic materials. *Mater. Sci. Eng. A* **278**, 36–45 (2000)
- Ewen, J.P., Spikes, H.A., Dini, D.: Contributions of molecular dynamics simulations to elastohydrodynamic lubrication. *Tribol. Lett.* **69**, 24 (2021)
- Bair, S., Vergne, P., Kumar, P., Poll, G., Krupka, I., Hartl, M., Habchi, W., Larsson, R.: Comment on “history, origins and prediction of elastohydrodynamic friction” by spikes and jie. *Tribol. Lett.* **58**(1), 1–8 (2015)
- Eyring, H.: Viscosity, plasticity, and diffusion as examples of absolute reaction rates. *J. Chem. Phys.* **4**(4), 283–291 (1936)
- Spikes, H., Jie, Z.: History, origins and prediction of elastohydrodynamic friction. *Tribol. Lett.* **56**(1), 1–25 (2014)
- Spikes, H., Zhang, J.: Reply to the comment by Scott Bair, Philippe Vergne, Punit Kumar, Gerhard Poll, Ivan Krupka, Martin Hartl, Wassim Habchi, Roland Larson on “History, origins and prediction of elastohydrodynamic friction” by Spikes and Jie in *Tribology Letters*. *Tribol. Lett.* **58**, 1–6 (2015)
- H. A. Spikes (2016) Comment on: Rheology of an ionic liquid with variable Carreau exponent: A full picture by molecular simulation with experimental contribution, by nicolas voeltzel, philippe vergne, nicolas fillot, nathalie bouscharain, laurent joly, *tribology letters* (2016) 64:25. *Tribol. Lett.*, 65(2), April 2017
- Voeltzel, N., Vergne, P., Fillot, N., Bouscharain, N., Joly, L.: Rheology of an ionic liquid with variable Carreau exponent: a full picture by molecular simulation with experimental contribution. *Tribol. Lett.* **64**(2), 25 (2016)
- Nicolas Voeltzel, Philippe Vergne, Nicolas Fillot, Nathalie Bouscharain, and Laurent Joly. Reply to the “comment on ‘rheology of an ionic liquid with variable Carreau exponent: A full

- picture by molecular simulation with experimental contribution, ' by n. voeltzel, p. vergne, n. fillot, n. bouscharain, l. joly, tribology letters (2016) 64:25" by h. a. spikes. *Tribol. Lett.*, 65(2), April 2017
18. Carreau, P.J.: Rheological equations from molecular network theories. *Trans. Soc. Rheol.* **16**(1), 99–127 (1972)
 19. Prandtl, L.: Ein gedankenmodell zur kinetischen theorie der festen körper. *J. Appl. Math. Mech.* **8**(2), 85–106 (1928)
 20. Spikes, H., Tysoe, W.: On the commonality between theoretical models for fluid and solid friction, wear and tribochemistry. *Tribol. Lett.* **59**(1), 1–4 (2015)
 21. Bair, S.: Purported fragile-to-Arrhenius crossover in squalane. *Proc. Natl. Acad. Sci. U.S.A.* **114**(42), 8805–8806 (2017)
 22. Jadhao, V., Robbins, M.O.: Probing large viscosities in glassformers with nonequilibrium simulations. *Proc. Natl. Acad. Sci. U.S.A.* **114**(30), 7952–7957 (2017)
 23. Jadhao, V., Robbins, M.O.: Reply to Bair: crossover to Arrhenius behavior at high viscosities in squalane. *Proc. Natl. Acad. Sci. U.S.A.* **114**(42), 8807–8808 (2017)
 24. Lucas, P.: Fragile-to-strong transitions in glass forming liquids. *J. Non-Cryst. Solids* **557**, 119367 (2021)
 25. Daivis, P.J., Evans, D.J.: Comparison of constant pressure and constant volume nonequilibrium simulations of sheared model decane. *J. Chem. Phys.* **100**(1), 541–547 (1994)
 26. Sivebaek, I.M., Samoilov, V.N., Persson, B.N.J.: Effective viscosity of confined hydrocarbons. *Phys. Rev. Lett.* **108**(3), 036102 (2012)
 27. Lemarchand, C.A., Bailey, N.P., Todd, B.D., Daivis, P.J., Hansen, J.S.: Non-Newtonian behavior and molecular structure of Coee bitumen under shear flow: a non-equilibrium molecular dynamics study. *J. Chem. Phys.* **142**(24), 244501 (2015)
 28. Popov, V.L., Gray, J.A.T.: Prandtl-tomlinson model: history and applications in friction, plasticity, and nanotechnologies. *ZAMM* **92**(9), 683–708 (2012)
 29. Prentice, I.J., Liu, X., Nerushev, O.A., Balakrishnan, S., Pulham, C.R., Camp, P.J.: Experimental and simulation study of the high-pressure behavior of squalane and poly- α -olefins. *J. Chem. Phys.* **152**(7), 074504 (2020)
 30. Crook, A.W., Allibone, T.E.: The lubrication of rollers iv. Measurements of friction and effective viscosity. *Philos. Trans. R. Soc. Lond. Ser. A* **255**(1056), 281–312 (1963)
 31. Müser, M.H.: Shear thinning in the Prandtl model and its relation to generalized Newtonian fluids. *Lubricants* **8**(4), 38 (2020)
 32. Ruina, A.: Slip instability and state variable friction laws. *J. Geophys. Res. Solid Earth* **88**(B12), 10359–10370 (1983)
 33. Müser, M.H.: Velocity dependence of kinetic friction in the Prandtl-Tomlinson model. *Phys. Rev. B* **84**(12), 125419 (2011)
 34. Smith, E.D., Robbins, M.O., Cieplak, M.: Friction on adsorbed monolayers. *Phys. Rev. B* **54**(11), 8252–8260 (1996)
 35. Fisher, D.S.: Sliding charge-density waves as a dynamic critical phenomenon. *Phys. Rev. B* **31**(3), 1396–1427 (1985)
 36. Plimpton, S.: Fast parallel algorithms for short-range molecular dynamics. *J. Comput. Phys.* **117**(1), 1–19 (1995)
 37. Price, M.L., Ostrovsky, D., Jorgensen, W.L.: Gas-phase and liquid-state properties of esters, nitriles, and nitro compounds with the OPLS-AA force field. *J. Comput. Chem.* **22**(13), 1340–1352 (2001)
 38. Siu, S.W.I., Pluhackova, K., Böckmann, R.A.: Optimization of the opls-aa force field for long hydrocarbons. *J. Chem. Theory Comput.* **8**(4), 1459–1470 (2012)
 39. Todd, B.D., Daivis, P.J.: Nonequilibrium Molecular Dynamics: Theory. Algorithms and Applications, Cambridge University Press, Cambridge (2017)
 40. Lees, A.W., Edwards, S.F.: The computer study of transport processes under extreme conditions. *J. Phys. C* **5**(15), 1921 (1972)
 41. Nosé, S.: A molecular dynamics method for simulations in the canonical ensemble. *Mol. Phys.* **52**(2), 255–268 (1984)
 42. Hoover, W.G.: Canonical dynamics: equilibrium phase-space distributions. *Phys. Rev. A* **31**, 1695–1697 (1985)
 43. McEwen, E.: The effect of variation of viscosity with pressure on the load-carrying capacity of the oil film between gear-teeth. *J. Inst. Pet.* **38**(1), 646–672 (1952)
 44. Bair, S.: Choosing pressure-viscosity relations. *High Temp. High Pressures* **44**, 415–428 (2015)
 45. Kondratyuk, N.D., Pisarev, V.V., Ewen, J.P.: Probing the high-pressure viscosity of hydrocarbon mixtures using molecular dynamics simulations. *J. Chem. Phys.* **153**(15), 154502 (2020)
 46. Paluch, M., Dendzik, Z., Rzoska, S.J.: Scaling of high-pressure viscosity data in low-molecular-weight glass-forming liquids. *Phys. Rev. B* **60**, 2979–2982 (1999)
 47. Lacks, D.J.: Energy landscapes and the non-Newtonian viscosity of liquids and glasses. *Phys. Rev. Lett.* **87**, 225502 (2001)
 48. Lodge, A.S.: A network theory of flow birefringence and stress in concentrated polymer solutions. *Trans. Faraday Soc.* **52**, 120–130 (1956)
 49. Jadhao, V., Robbins, M.O.: Rheological properties of liquids under conditions of elastohydrodynamic lubrication. *Tribol. Lett.* **67**, 66 (2019)
 50. ZiyaAkcasu, A., Han, C.C.: Molecular weight and temperature dependence of polymer dimensions in solution. *Macromolecules* **12**(2), 276–280 (1979)
 51. Kok, C.M., Rudin, A.: Relationship between the hydrodynamic radius and the radius of gyration of a polymer in solution. *Rapid Commun.* **2**(11), 655–659 (1981)
 52. Qiu, X.H., Ediger, M.D.: Local and global dynamics of unentangled polyethylene melts by ^{13}C nmr. *Macromolecules* **33**(2), 490–498 (1999)